Supplementary Information: Bridging the Gap Between Microstructurally Resolved Computed Tomography-Based and Homogenised Doyle-Fuller-Newman Models for Lithium-Ion Batteries

E. C. Tredenick*[1,6], A. M. Boyce[2,3,6], S. Wheeler[4,6], J. Li[2,6], Y. Sun[4,6], R. Drummond[5], S. R. Duncan[1,6], P. S. Grant[4,6] and P. R. Shearing[1,2,6]

[1]Department of Engineering Science, University of Oxford, Oxford, OX1 3PJ, UK
[2]Electrochemical Innovation Lab, Department of Chemical Engineering, University College London, London, WC1E 7JE, UK
[3]School of Mechanical and Materials Engineering, University College Dublin, Dublin, Ireland
[4]Department of Materials, University of Oxford, Oxford, OX1 3PH, UK
[5]Department of Automatic Control and Systems Engineering, University of Sheffield, Sheffield, S1 3JD, UK
[6]The Faraday Institution, Quad One, Harwell Campus, Didcot, OX11 0RA, UK

Doyle-Fuller-Newman Model Framework

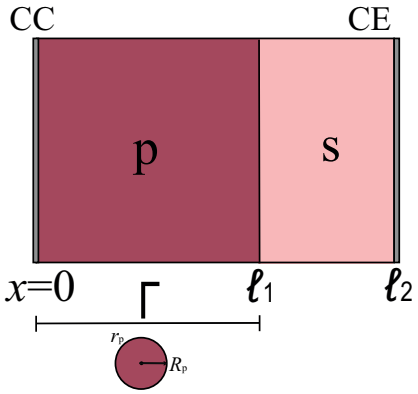

Figure S1: The model half cell battery domain. The separator, s, and positive cathode compartment, p, is shown. The cathode domain, Γ, that excludes the separator, current collector (CC) and lithium metal plate counter electrode (LMP) are shown. ℓ_1 is the thickness of the cathode and ℓ_2 is the thickness of the entire half cell.

The model equations[2] are shown below, on the domain Γ, except for the separator, $I_{\text{sign}} = -1$ for discharge, and $t > 0$:

$$\frac{\partial c_{\text{s,p}}}{\partial t} = \frac{1}{r_{\text{p}}^2}\frac{\partial}{\partial r_{\text{p}}}\left(r_{\text{p}}^2\, D_{\text{s,p}}\frac{\partial c_{\text{s,p}}}{\partial r_{\text{p}}}\right), 0 < r_{\text{p}} < R_{\text{p}}, \tag{S1a}$$

$$-\frac{\partial}{\partial x}\left(-\sigma_{\text{s,p}}\frac{\partial \phi_{\text{s,p}}}{\partial x}\right) = a_{\text{p}}\, i_{\text{BV}}, \tag{S1b}$$

$$\varepsilon_{\text{e,p}}\frac{\partial c_{\text{e,p}}}{\partial t} = -\frac{\partial}{\partial x}\left(-D_{\text{e,p}}\frac{\partial c_{\text{e,p}}}{\partial x}\right) + \frac{\left(1-t^{+}\right)\, a_{\text{p}}\, i_{\text{BV}}}{F}, \tag{S1c}$$

$$\varepsilon_{\text{e,s}}\frac{\partial c_{\text{e,s}}}{\partial t} = -\frac{\partial}{\partial x}\left(-D_{\text{e,s}}\frac{\partial c_{\text{e,s}}}{\partial x}\right), \ell_1 < x < \ell_2, \tag{S1d}$$

$$\frac{\partial}{\partial x}\left[\kappa_{\text{e,p}}\left(-\frac{\partial \phi_{\text{e,p}}}{\partial x} + \omega\,\frac{\partial(\ln(c_{\text{e,p}}))}{\partial x}\right)\right] = a_{\text{p}}\, i_{\text{BV}}, \tag{S1e}$$

$$\frac{\partial}{\partial x}\left[\kappa_{\text{e,s}}\left(-\frac{\partial \phi_{\text{e,s}}}{\partial x} + \omega\,\frac{\partial(\ln(c_{\text{e,s}}))}{\partial x}\right)\right] = 0, \quad \ell_1 < x < \ell_2, \tag{S1f}$$

$$\omega = \frac{2\, g\, \left(1-t^{+}\right)\, R\, T}{F}, \tag{S1g}$$

*Email: eloise.tredenick@eng.ox.ac.uk

with boundary conditions as follows:

$$\left.\frac{\partial c_{\mathrm{s,p}}}{\partial r_{\mathrm{p}}}\right|_{r_{\mathrm{p}}=0} = 0, \tag{S2a}$$

$$-D_{\mathrm{s,p}}\left.\frac{\partial c_{\mathrm{s,p}}}{\partial r_{\mathrm{p}}}\right|_{r_{\mathrm{k}}=R_{\mathrm{p}}} = \frac{i_{\mathrm{BV}}(R_{\mathrm{p}},x,t)}{F}, \tag{S2b}$$

$$-\sigma_{\mathrm{s,p}}\left.\frac{\partial \phi_{\mathrm{s,p}}}{\partial x}\right|_{x=0} = I\ I_{\mathrm{sign}}, \tag{S3a}$$

$$\left.\frac{\partial \phi_{\mathrm{s,p}}}{\partial x}\right|_{x=\ell_1} = 0, \tag{S3b}$$

$$\left.\frac{\partial c_{\mathrm{e,p}}}{\partial x}\right|_{x=0} = 0, \tag{S4a}$$

$$c_{\mathrm{e,p}}(\ell_1,t) = c_{\mathrm{e,s}}(\ell_1,t), \tag{S4b}$$

$$-D_{\mathrm{e,s}}\left.\frac{\partial c_{\mathrm{e,s}}}{\partial x}\right|_{x=\ell_1} = -D_{\mathrm{e,p}}\left.\frac{\partial c_{\mathrm{e,p}}}{\partial x}\right|_{x=\ell_1}, \tag{S4c}$$

$$-D_{\mathrm{e,s}}\left.\frac{\partial c_{\mathrm{e,s}}}{\partial x}\right|_{x=\ell_2} = \frac{\left(1-t^{+}\right)\ I\ I_{\mathrm{sign}}}{F}. \tag{S4d}$$

$$\left.\frac{\partial \phi_{\mathrm{e,p}}}{\partial x}\right|_{x=0} = 0, \tag{S5a}$$

$$\phi_{\mathrm{e,p}}(\ell_1,t) = \phi_{\mathrm{e,s}}(\ell_1,t), \tag{S5b}$$

$$\kappa_{\mathrm{e,s}}\left.\frac{\partial \phi_{\mathrm{e,s}}}{\partial x}\right|_{x=\ell_1} = \kappa_{\mathrm{e,s}}\ \omega\ \left.\frac{\partial(\ln(c_{\mathrm{e,s}}))}{\partial x}\right|_{x=\ell_1} - I\ I_{\mathrm{sign}}, \tag{S5c}$$

$$\text{Reference Potential: } \phi_{\mathrm{e,s}}(\ell_2,t) = 0, \tag{S5d}$$

$$\tag{S5e}$$

and initial conditions:

$$c_{\mathrm{s,p}}(r_{\mathrm{p}},0) = c_{\mathrm{s,p,0}}, \tag{S6a}$$

$$\phi_{\mathrm{s,p}}(x,0) = U_{\mathrm{k}}, \tag{S6b}$$

$$c_{\mathrm{e,k}}(x,0) = c_{\mathrm{e0}},\ \ \mathrm{k}\in\{\mathrm{p,s}\}, \tag{S6c}$$

$$\phi_{\mathrm{e,k}}(x,0) = 0,\ \ \mathrm{k}\in\{\mathrm{p,s}\}, \tag{S6d}$$

and auxiliary equations:

$$a_{\mathrm{p}} = \frac{3\ (1-\varepsilon_{\mathrm{e,p}}-\varepsilon_{\mathrm{CBD,p}})}{R_{\mathrm{p}}}, \tag{S7a}$$

$$i_{\mathrm{BV}} = 2\ i_0\ \sinh\left(\frac{F\ \eta_{\mathrm{p}}}{2\ R\ T}\right), \tag{S7b}$$

$$i_0 = k_{\mathrm{p}}\ F\ \sqrt{c_{\mathrm{e,p}}\ c_{\mathrm{s,p}}\left(c_{\mathrm{s,p,max}}-c_{\mathrm{s,p}}\right)}\Big|_{r_{\mathrm{p}}=R_{\mathrm{p}}}, \tag{S7c}$$

$$\eta_{\mathrm{p}} = \phi_{\mathrm{s,p}}-\phi_{\mathrm{e,p}}-U_{\mathrm{p}}|_{r_{\mathrm{p}}=R_{\mathrm{p}}}, \tag{S7d}$$

$$D_{\mathrm{e,k}}(c_{\mathrm{e,k}}) = D_{\mathrm{e,bulk}}(c_{\mathrm{e,k}})\ \varepsilon_{\mathrm{e,k}}{}^{\,b_{\mathrm{k}}},\ \ \mathrm{k}\in\{\mathrm{p,s}\}, \tag{S7e}$$

$$\kappa_{\mathrm{e,k}}(c_{\mathrm{e,k}}) = \kappa_{\mathrm{e,bulk}}(c_{\mathrm{e,k}})\ \varepsilon_{\mathrm{e,k}}{}^{\,b_{\mathrm{k}}},\ \ \mathrm{k}\in\{\mathrm{p,s}\}, \tag{S7f}$$

$$V = \phi_{\mathrm{s,p}}(0,t)+R_{\mathrm{c}}\ I\ I_{\mathrm{sign}}, \tag{S7g}$$

where solved variables are shown in Table S1. The bulk electrolyte diffusivity, $D_{\mathrm{e,bulk}}$, and conductivity, $\kappa_{\mathrm{e,bulk}}$, are shown as functions of the electrolyte concentration, c_{e} and are found[4] by fitting polynomials to available data,[5] producing R^2 values of 99.99% and 99.97%:

$$D_{\mathrm{e,bulk}}(c) = -7.55\times10^{-21}\ c^3+8.231\times10^{-17}\ c^2-3.401\times10^{-13}\ c+5.464\times10^{-10}, \tag{S8}$$

$$\kappa_{\mathrm{e,bulk}}(c) = 5.746\times10^{-18}\ c^5-1.025\times10^{-13}\ c^4+7.082\times10^{-10}\ c^3-2.236\times10^{-6}\ c^2+0.00273\ c-0.003, \tag{S9}$$

where c is $c_{\mathrm{e,k,i}}$.

The open circuit potential (OCP) function for NMC622 is as follows:

$$U_{\mathrm{p1}}(x) = a_1\ \exp\left(-((x-b_1)/c_1)^2\right)+a_2\ \exp\left(-((x-b_2)/c_2)^2\right)+a_3\ \exp\left(-((x-b_3)/c_3)^2\right)+ a_4\ \exp\left(-((x-b_4)/c_4)^2\right)+a_5\ \exp\left(-((x-b_5)/c_5)^2\right), \tag{S10}$$

where x is $c_{\mathrm{p1}}/c_{\mathrm{p1}}^{\mathrm{max}}$, and

$$a_1=5.207,\ b_1=-0.2483,\ c_1=0.9933,\ a_2=-1.068,\ b_2=0.7811,\ c_2=0.1661,\ a_3=4.191,\ b_3=0.7332,$$
$$c_3=0.289,\ a_4=0.2152,\ b_4=0.9318,\ c_4=0.06901,\ a_5=-1.867,\ b_5=0.633,\ c_5=0.2105,$$

and is formulated by fitting to the experimental data,[4] by first normalising the data from [0, 1] to [0.27, 0.91] to account for the stoichiometry, then using a 5 term Gaussian function with an R-squared value of 99.99%, and should be utilised only with the attached MATLAB code due to sensitivities of significant figures. The LFP OCP[3] is as follows:

$$U_{\mathrm{p2}}(y) = 3.382 + 0.0047\, y + 1.627\, \exp\left(-81.163\, y^{1.0138}\right) + 7.6445 \times 10^{-8}\, \exp\left(25.36\, y^{2.469}\right) - 8.441 \times 10^{-8}\, \exp\left(25.262\, y^{2.478}\right), \tag{S11}$$

where y is $c_{\mathrm{p2}}/c_{\mathrm{p2}}^{\mathrm{max}}$.

Table S1: Variables of the DFN model, where k $\in$ {p,s}, for positive and separator compartments.

Parameter	Description	Unit
a_{p}	Reaction surface area per volume	1/m
$c_{\mathrm{e,k}}$	Concentration of lithium in the liquid electrolyte	mol/m^3
$c_{\mathrm{s,p}}$	Concentration of lithium in the solid particles	mol/m^3
$D_{\mathrm{e,k}}$	Diffusivity function in the electrolyte	m^2/s
$D_{\mathrm{e,bulk}}$	Bulk diffusivity function in the electrolyte	m^2/s
i_{BV}	Butler-Volmer reaction density	A/m^2
i_0	Exchange current density	A/m^2
r_{p}	Particle radius	m
t	Time	s
U_{p}	Open circuit potential (OCP)	V
V	Voltage	V
x	Direction through cell	m
$\kappa_{\mathrm{e,k}}$	Ionic conductivity function in the electrolyte	S/m
$\kappa_{\mathrm{e,bulk}}$	Bulk ionic conductivity function in the electrolyte	S/m
η_{p}	Local overpotential	V
$\phi_{\mathrm{s,p}}$	Potential in the solid particles	V
$\phi_{\mathrm{e,k}}$	Potential in the liquid electrolyte	V

CT Image-based Model Framework

Diffusion based on Fick's first and second laws, together with ion conduction and conservation of current associated with lithium-ion transport are modelled as follows:

$$J_{\mathrm{e}} = -D_{\mathrm{e,p}} \nabla c_{\mathrm{e,p}} + \frac{i_{\mathrm{e}} t^{+}}{F}, \tag{S12a}$$

$$\frac{\partial c_{\mathrm{e,p}}}{\partial t} + \nabla \cdot J_{\mathrm{e}} = 0, \tag{S12b}$$

$$i_{\mathrm{e}} = -\kappa_{\mathrm{e,p}} \nabla \phi_{\mathrm{e,p}} + \frac{2g\kappa_{\mathrm{e,p}} RT}{F} (1 - t^{+}) \nabla \ln c_{\mathrm{e,p}}, \tag{S12c}$$

$$\nabla \cdot i_{\mathrm{e}} = 0. \tag{S12d}$$

The corresponding diffusion for solid lithium transport and Ohm's law with charge conservation for electronic conduction in the active material are:

$$J_{\mathrm{p}} = -D_{\mathrm{s,p}} \nabla c_{\mathrm{s,p}}, \tag{S13a}$$

$$\frac{\partial c_{\mathrm{s,p}}}{\partial t} + \nabla \cdot J_{\mathrm{p}} = 0, \tag{S13b}$$

$$i_{\mathrm{p}} = -\sigma_{\mathrm{s,p}} \nabla \phi_{\mathrm{s,p}}, \tag{S13c}$$

$$\nabla \cdot i_{\mathrm{p}} = 0. \tag{S13d}$$

Ohm's law and charge conservation for electronic conduction in the carbon binder domain are given as follows for NMC. For LFP, the carbon-binder and electrolyte domains are homogenised using Bruggeman exponents with equations similar to the DFN model.

$$i_{\mathrm{c}} = -\sigma_{\mathrm{CBD}} \nabla \phi_{\mathrm{c}}, \tag{S14a}$$

$$\nabla \cdot i_{\mathrm{c}} = 0. \tag{S14b}$$

The boundary conditions are as follows, related to Fig. 2

$$\mathbf{i}_c \cdot \mathbf{n}_{cc} = i_{in}|_{z=0}, \tag{S15a}$$

$$\mathbf{J}_e \cdot \mathbf{n}_e = \left.\frac{i_{in}}{F}\right|_{z=t_{cc}+L+t_{sep}}, \tag{S15b}$$

$$\mathbf{i}_e \cdot \mathbf{n}_e = -i_{in}|_{z=t_{cc}+L+t_{sep}}, \tag{S15c}$$

$$\phi_{e,p} = 0|_{z=t_{cc}+L+t_{sep}}, \tag{S15d}$$

$$\mathbf{i}_c \cdot \mathbf{n}_{se} = 0|_{z=t_{cc}+L}, \tag{S15e}$$

$$\mathbf{i}_p \cdot \mathbf{n}_{se} = 0|_{z=t_{cc}+L}, \tag{S15f}$$

$$\mathbf{J}_e \cdot \mathbf{n}_{pe} = \frac{-i_{BV}}{F}, \tag{S15g}$$

$$\mathbf{J}_s \cdot \mathbf{n}_{pe} = \left.\frac{-i_{BV}}{F}\right|_{r=R_p}, \tag{S15h}$$

$$\mathbf{i}_e \cdot \mathbf{n}_{pe} = -i_{BV}, \tag{S15i}$$

$$\mathbf{i}_p \cdot \mathbf{n}_{pe} = i_{BV}|_{r=R_p}. \tag{S15j}$$

The charge transfer reaction is represented using the Butler-Volmer equation with an exchange current density as described in equations (S7b) to (S7d), voltage and electrolyte functions as described in equations (S7e) to (S7g) and initial conditions the same as equations S6.

NMC622 Experimental Validation Including Models

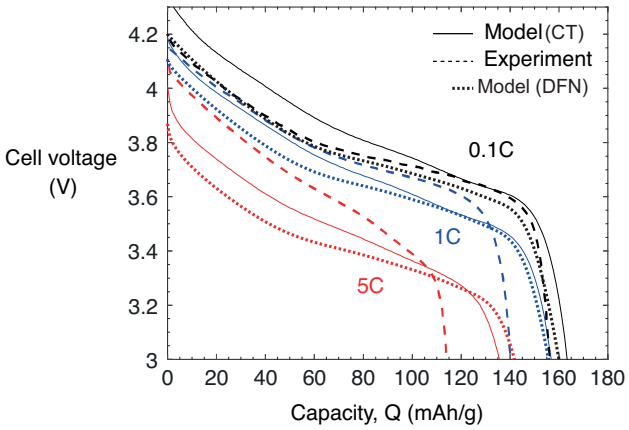

Figure S2: Voltage profile with capacity for NMC622. The experimental data and original fitted CT model (re-used and edited with permission[1]) is shown, along with the new DFN modelling fit. The experimental data is dashed line, the CT model is the solid line and the DFN model is shown as dotted. The same parameters for the DFN model as already described in Table4 are used, except due to the experimental setup with electrode thickness of 40 μm, volume fraction of 0.35, applied current of 1.8×10^{-5} mA and cell weight of 1×10^{-7} g.

Li Particle Concentration for LFP

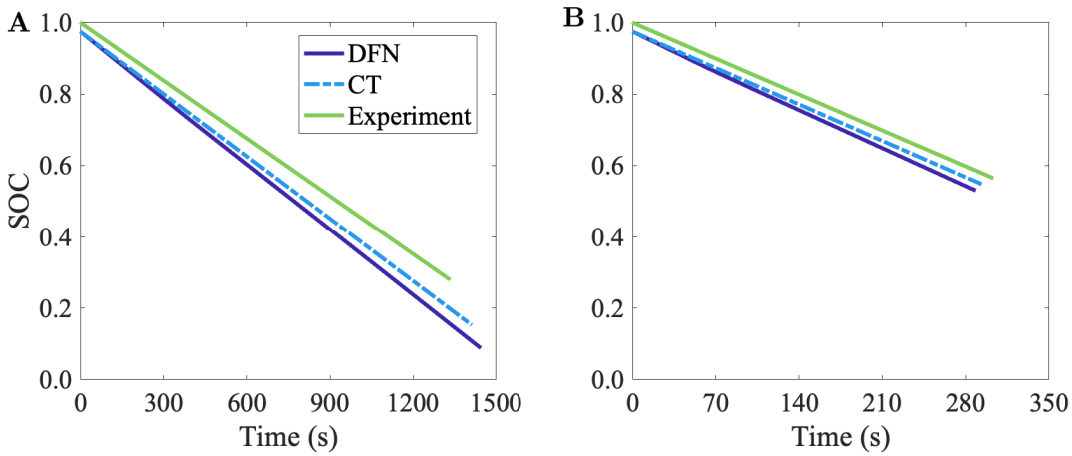

Figure S3: The LFP state-of-charge (SOC) with time, where the SOC is the solid particle concentration integrated over the particle radius and cathode, at (A) 2C and (B) 5C, where $\text{SOC}(t) = \frac{3}{L_p R_p^3} \int_0^{L_p} \int_0^{R_p} r_p^2 \left(1 - c_{s,p}(r_p, x_p, t)/c_{s,p,max}\right) dr_p dx_p$.

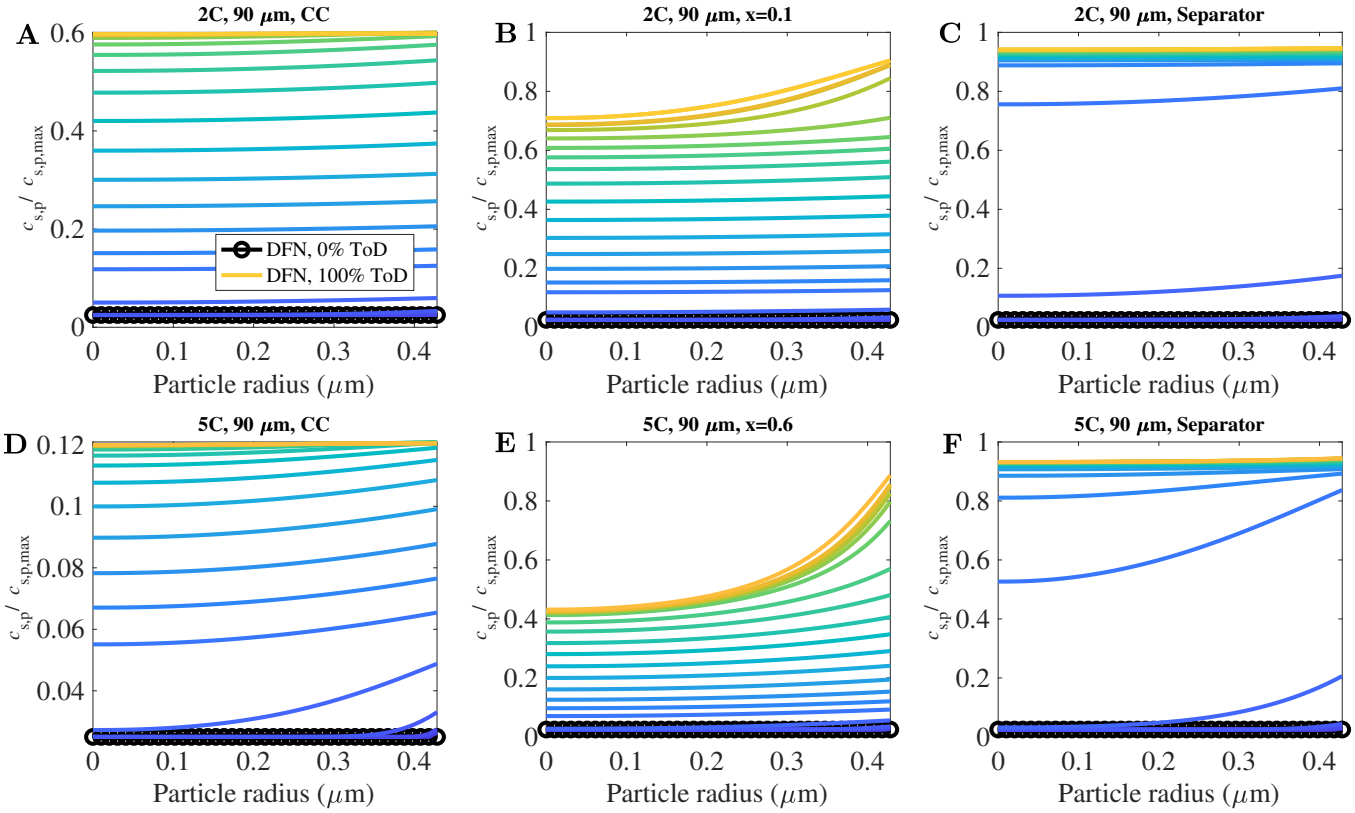

Figure S4: 2C (A, B, C) and 5C (D, E, F), 90 μm for LFP simulation results for the DFN model. The normalised Li concentration in the active particles ($c_{s,p}/c_{s,p,max}$) is plot as a function of particle radius. Three points along the electrode are shown in each column including near the CC (A, D), in (B,E) near the centre of the electrode (10% and 60% through) near the 'S' shapes in Fig.5), and near the separator (C, F). Note the y-axis scales are different in (A) and (D) compared to the other plots.

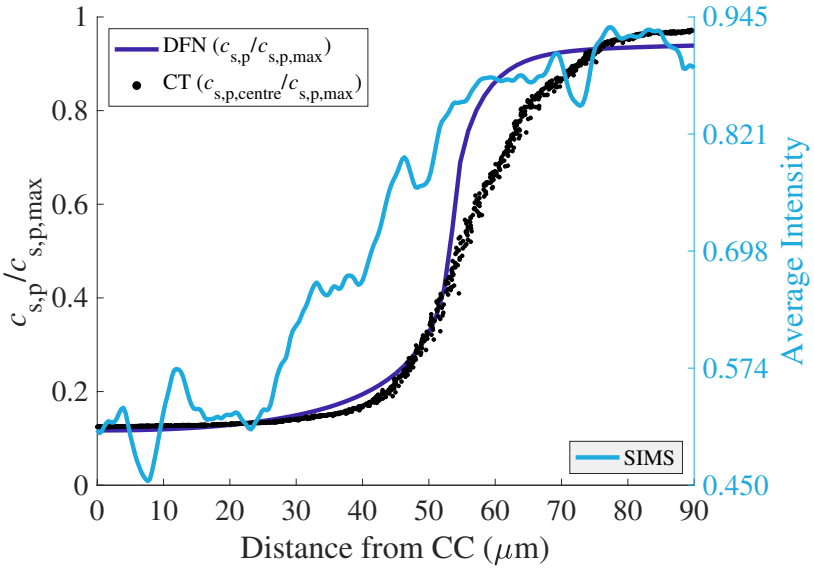

Figure S5: Comparison of Fig. 8 within the one figure, for the concentration of Li ions in the simulations of the DFN and CT models, along with the SIMS results for qualitative comparison noting the two different y-axes (SIMS on the right hand side). Note the DFN results are integrated over the particle radius ($c_{s,p}/c_{s,p,max}$), the CT results are at the centre of the particle ($c_{s,p,centre}/c_{s,p,max}$) and the SIMS is the average intensity.

References

[1] Adam M Boyce, Xuekun Lu, Dan JL Brett, and Paul R Shearing. Exploring the influence of porosity and thickness on lithium-ion battery electrodes using an image-based model. *Journal of Power Sources*, 542:231779, 2022.

[2] Marc Doyle, Thomas F Fuller, and John Newman. Modeling of galvanostatic charge and discharge of the lithium/polymer/insertion cell. *Journal of The Electrochemical Society*, 140(6):1526, 1993.

[3] Ali Ghorbani Kashkooli, Siamak Farhad, Dong Un Lee, Kun Feng, Shawn Litster, Siddharth Komini Babu, Likun Zhu, and Zhongwei Chen. Multiscale modeling of lithium-ion battery electrodes based on nano-scale X-ray computed tomography.

Journal of Power Sources, 307:496–509, 3 2016.

[4] EC Tredenick, S Wheeler, R Drummond, Y Sun, SR Duncan, and PS Grant. A multilayer Doyle-Fuller-Newman model to optimise the rate performance of bilayer cathodes in Li ion batteries. https://doi.org/10.21203/rs.3.rs-3906430/v2. (pre-print).

[5] Lars Ole Valøen and Jan N Reimers. Transport Properties of LiPF6-Based Li-Ion Battery Electrolytes. *Journal of The Electrochemical Society*, 152:A882, 2005.